Article

Evolution of Microstructure during Isothermal Treatments of a Duplex-Austenitic 0.66C11.4Mn.9.9Al Low-Density Forging Steel and Effect on the Mechanical Properties

Idurre Kaltzakorta [1,*], Teresa Gutierrez [1], Roberto Elvira [2], Pello Jimbert [3] and Teresa Guraya [3]

1 TECNALIA, Basque Research and Technology Alliance (BRTA), Parque Científico y Tecnológico de Bizkaia, C/Astondoa, Edificio 700, 48160 Derio, Spain; Teresa.Gutierrez@tecnalia.com
2 Sidenor I+D, Barrio Ugarte s/n, 48970 Basauri, Spain; Roberto.Elvira@sidenor.com
3 Faculty of Engineering in Bilbao, University of the Basque Country UPV/EHU, Paseo Rafael Moreno "Pitxitxi" 3, 48003 Bilbao, Spain; Pello.Jimbert@ehu.eus (P.J.); Teresa.Guraya@ehu.eus (T.G.)
* Correspondence: Idurre.Kaltzakorta@tecnalia.com

Abstract: In the last decades, low-density steels for forging have increasing interest in the automotive industry, and good mechanical properties are required for their real application. This paper describes the results obtained for a 0.66C11.4Mn9.9Al duplex austenitic low-density steel after applying a set of isothermal treatments at different combinations of time and temperature, aimed to promote kappa carbide precipitation, and improve the mechanical properties obtained with a water quenching treatment. The effects of the different isothermal treatments on the microstructure and on the mechanical properties have been analyzed and compared to those obtained from a quenching heat treatment. We found that isothermal treatments in the range temperature between 550–750 °C promoted the profuse precipitation of coarse kappa carbides at grain boundaries, which dramatically reduced the ductility of the alloy, whereas a traditional quenching treatment resulted in a better combination of ductility and mechanical strength.

1. Introduction

To comply with the severe policies regarding CO_2 emissions, the automotive industry is focused on reducing the weight of cars without penalizing the safety of passengers (a reduction of 100 kg in the vehicle weight implies ~8.5 g less CO_2 emissions per km).

For this purpose, they are adopting different strategies such as the redesign of components (to eliminate unnecessary material), the use of high-strength steels (to reduce thickness) and the reduction of the density of the material used. In the literature, many studies have focused on the development of lightweight steels with a high strength and low density [1–3], the Fe-Mn-Al-C system being the most widely explored. Low-density steels that consider additions of Al (more than 10%), obtaining a density reduction of around 15%, are the most studied ones [3]. Depending on the chemical composition (weight %), low-density steels can be classified into three different categories [4]: austenitic steels (0.5 < %C < 2, 8 < %Al < 12, 15 < %Mn < 30), duplex steels (0.1 < %C < 0.7, 3 < %Al < 10, 5 < %Mn < 30) and ferritic steels (%C < 0.03, 5 < %Al < 8, %Mn < 8); Mn and C are the austenite former while Al is the strong ferrite former. Therefore, the mechanical properties of the Fe–Mn–Al–C system are dependent on the deformation characteristics of the constituent phase(s) [5].

A promising improvement for these low-density alloys comes from the proper precipitation of kappa carbides (k-carbide). The k-carbide is a carbide with an L1′$_2$-type structure with a perfect formula of (Fe,Mn)$_3$AlC, and the lattice parameters vary with the C and Mn content [6]. The addition of aluminium accelerates the precipitation of ordered perovskite

structure carbide, i.e., k-carbide [1,7–9]. Even if in the beginning, k-carbide was thought to be harmful to ductility [10–12], it has recently been documented that k-carbide can enhance strength and ductility at the same time by optimizing its morphology, distribution, fraction and size [13,14]. For the enhancement of mechanical properties, the intragranular nanosized k-carbides are usually desirable, whereas the intergranular k-carbide must be avoided [13]. In a ferritic Fe-3.0Mn-3.0Al-0.3C (wt.%) alloy, the same author described that lamellar-type k-carbides were formed as a result of a eutectoid reaction during isothermal annealing between 500 °C and 600 °C associated with nucleation and growth. For austenitic low-density alloys with a high-Mn content, in aging treatments between 500 °C and 600 °C, rectangular-shaped k-carbides were reported to precipitate out, mainly from the austenitic matrix via spinodal decomposition during aging [13–16].

In a previous work [17], we carried out a preliminary study of several low-density steels formed by ferritic, austenitic and duplex microstructures. For this investigation, a 0.66C11.4Mn9.9Al duplex austenitic low-density steel was selected to be submitted to a set of isothermal treatments at different combinations of time and temperature, aimed to promote kappa carbide precipitation in order to study the influence of this k-carbide precipitation on the final mechanical properties and to define an appropriate isothermal heat treatment for obtaining a good combination of strength and ductility for forged components. First, the kinetics of k-carbide precipitation under different isothermal conditions was studied. Samples were quenched from 1150 °C and isothermally heat-treated by varying the treatment temperature in the range of 550–750 °C and the holding time in the range of 0.5–5 h. Second, tensile tests were carried out to study the effect of the k-carbide precipitation on the final mechanical properties of the treated materials, and the results were compared to those obtained for the same material after water quenching.

2. Materials and Methods

The selected duplex low-density steel with the theoretical composition of 0.65C12Mn10Al (wt.%) was melted in a vacuum levitation furnace using iron pieces (99.97+%), graphite flakes (99.9%), manganese pieces (99.9%) and pure aluminium pieces (99%+) as raw materials. The advantage of this equipment is that it works in a protective atmosphere, which eliminates risks of contamination and therefore yields a pure and reproducible cast material that also allows for remelting. To ensure the homogeneous distribution of the composition throughout the ingot, two refusions were performed, and ingots of about 1 kg were cast. In Figure 1a the cylindrical cast ingot is shown, whereas Figure 1b corresponds to the bar forged from the same ingot.

Figure 1. (**a**) Ingot cast in the levitation vacuum furnace and (**b**) bar forged from the ingot.

Two analytical techniques were used to determine the actual composition of the cast alloy. The C content was analyzed by Infra-Red (IR) detection after a sample combustion using an IR LECO CS-400 (LECO- St. Joseph, MI, USA). The Al and Mn contents were determined by plasma emission spectrometry (ICP-OES) in a THERMO-ICAP 7400 DUO equipment (Thermofisher Scientific, Waltham, MA, USA). The sample was dissolved in a mixture of nitric and clorhydric acids (1:3). Then, the solution was filtered, and the residue was collected. The filtrate was made up to the mark with Milli-Q water. The residue

was calcined at 550 °C, melted at 950 °C in lithium metaborate and dissolved in an acid medium for further analysis. The final composition is the sum of the contents obtained by analyzing the acid-soluble and the acid-insoluble parts. Four samples were extracted from different areas of the outer and the inner parts of the ingot from the upper and lower sides, in order to analyze the homogeneity of the ingot, obtaining a similar composition (standard deviation values of 0.005 for the carbon, 0.05 for the aluminium and 0.09 for the manganese were obtained).

The ingots were forged using a mechanical hammer. A ThermoCalc (Thermocalc®Sofware version 2020a, database TCFe6)phase diagram of the cast alloy was used to determine the forging conditions based on the temperature range, where the highest fraction of austenite, appropriate for hot working, was expected (Figure 2). During the forging process, to keep the material in the temperature range where austenite was the dominant phase, and considering that the ingots cool down very fast during manipulation, the ingots were heated up to 1150 °C, and when the temperature dropped below 900 °C they were heated again until the entire bar was forged. A Land Ametek Cyclops L Series Digital Pyrometer (Land Instruments International Ltd, Dronfield, UK) was used in all cases to control the ingot temperature. The average reduction that was applied was in the range of 50–65%, from an initial 30-mm diameter to about 11–15 mm at the end of the process (Figure 1b).
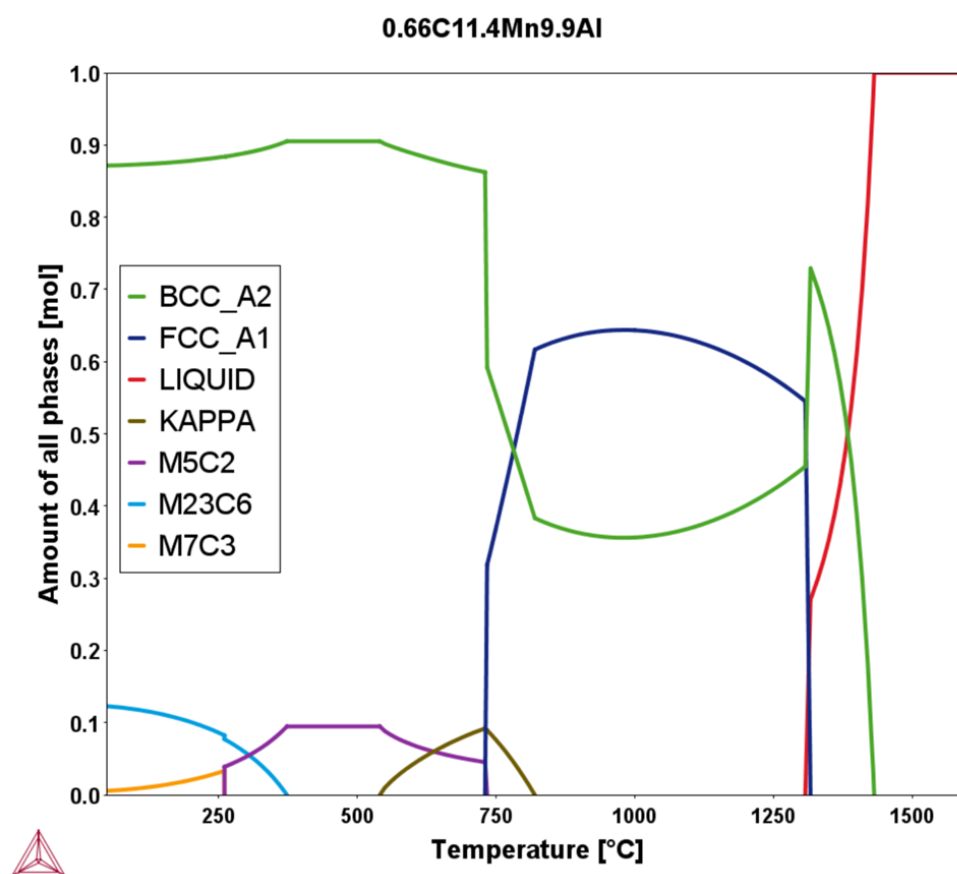

Figure 2. Phase diagram of the analyzed composition calculated with ThermoCalc®software (version 2020a, TCFe6 Database).

The density of the cast alloy was measured by calculating the density of the sample by measuring the mass of the sample both in air and immerged in a liquid of known density using a Radwag AS 120.X2 PLUS analytical balance (Radwag, Radom, Poland) with an accuracy of 0.01 mg. The density of the sample ρ_s (in g·cm^{-3}) was calculated using Equation (1):

$$\rho_s = \frac{m_a}{m_a - m_l} \cdot \rho_l \tag{1}$$

where m_l is the mass of the sample in the liquid, m_a is the mass of the sample in air (g), and ρ_l is the density of the liquid (g·cm^{-3}). In all cases, the liquid water and its density were considered to be 1 g·cm^{-3} regardless of the temperature.

For the microstructural characterization, the samples were sectioned, mechanically grinded and polished to up to 0.05 microns γ-Al$_2$O$_3$, and etched with 5% Nital solution. Microstructures were studied in Leica DM 400 (LEICA, Wetzlar, Germany) and Zeiss AxioCamMRc5 (ZEISS, Jena, Germany) optical microscopes and a FEI Quanta 450 (FEI, Hillsboro, OR, USA) field-emission scanning electron microscope (FEG-SEM) operating at 20 kV. The FEG-SEM was equipped with an energy dispersive spectrometer (EDS) and EBSD detector. Samples were also analyzed by X-ray diffraction (XRD) in a Rigaku DMAX-RB X-ray diffractometer (Rigaku Europe SE, Neu-Isenburg, Germany) with a Cu target operating at 40 kV and 150 mA.

Dilatometry studies were carried out using a Dilatometer BAHR 805L (TAInstruments, New Castle, DE, USA). In a vacuum chamber, the sample was located between quartz rods and heated inside an induction coil. The temperature was controlled by an RhPt thermocouple, and the sample dilatation was measured by a linear variable displacement transducer (LVDT). Sample cooling was carried out by blowing an argon or helium flow, depending on the required cooling rate. Heat treatments were performed in a Carbolite Wire Wound Tube Furnace TZF 12/65/550 (Nabertherm GmbH, Lilienthal, Germany) with temperature and atmosphere control. Finally, an Instron Machine, Model 5500R (INSTRON; Barcelona, Spain), was used to carry out the tensile tests.

3. Results and Discussion

The actual chemical composition of the steel was a 11.4 wt.% Mn, 9.9 wt.% Al, 0.66 wt.% C and Fe balance. The measured density of 6.86 g/cm^3 was in good agreement with the theoretical value of 6.80 g/cm^3, calculated with ThermoCalc software. The cast low-density steel resulted in being 13% lighter than pure iron.

3.1. Microstructural Evolution in Heat Treatments

3.1.1. Starting Microstructure

As the material was forged at 1150 °C, the microstructure at this temperature was defined as the initial condition to study the microstructural changes and, particularly, the k-carbide precipitation during different isothermal heat treatments. To analyze these changes, several samples of the alloy were heated up to 1150 °C at a heating rate of 5 °C/min, kept at that temperature for an extra 30 min and then water-quenched. According to the ThermoCalc diagram (Figure 2), the expected duplex microstructure would be formed by 38% ferrite and 62% austenite. Figure 3 shows the microstructure of the quenched samples. The optical microscope image shows a homogeneous duplex microstructure (Figure 3a) formed by austenite (darker regions) and ferrite (lighter regions). The volume fraction of each phase was calculated by an automatic image analysis performed on low magnification images according to ASTM E562-08 [18]. The calculated results were 37% ferrite and 63% austenite. Both phases were also confirmed as ferrite and austenite by SEM-EBSD (Figure 3b,c). The phase proportion measured on the EBSD map was a 65% area for austenite and a 35% area for ferrite. Although the EBSD results correspond to the area % of a reduced area and the ThermoCalc results correspond to the volume %, both are in good agreement with the volume fraction of each phase measured by point counting. X-ray diffraction (XRD) was used to confirm whether k-carbides were formed during quenching. The diffractogram shown in Figure 3d confirms the presence of the FCC and BCC structures by the peaks at (2θ) values of 42.5° and 44.3°, respectively. There was no evidence of the k-carbide peak, which was expected to be at 40.6°.
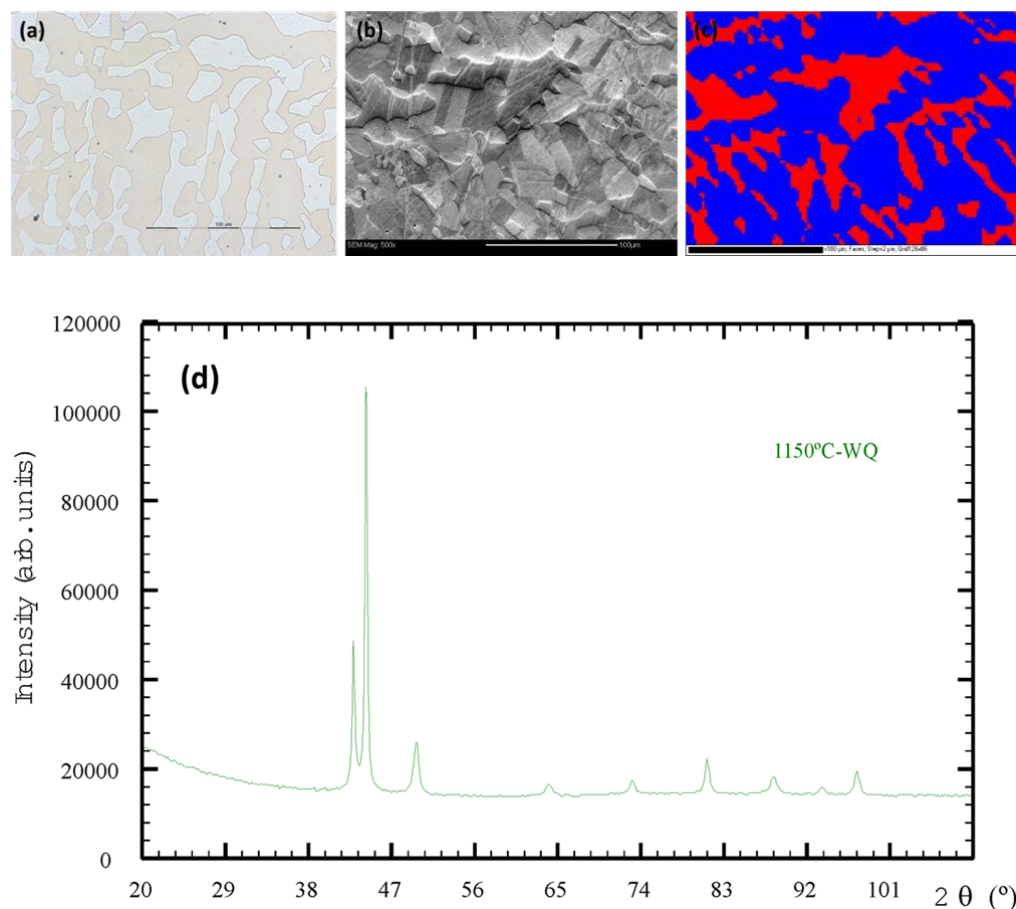
Figure 3. Microstructure images obtained by (**a**) optical microscope, (**b**) SEM image and (**c**) its corresponding phase EBSD mapping (ferrite in red and austenite in blue) of the sample that was water-quenched from 1150 °C, and (**d**) its XRD diffractogram.

3.1.2. Phase Transformation and K-Carbide Precipitation

A dilatometry test was carried out on a sample quenched from 1150 °C in order to observe the transformations that took place during heating and cooling. Heating from room temperature to 1000 °C was conducted at 0.05 °C/s, and reverse cooling to room temperature was conducted at 0.01 °C/s. Figure 4 shows the dilatometry curves and their derivative, corresponding to the heating (Figure 4a) and the cooling (Figure 4b) transformations. In the heating curve, the peak observed at 500 °C can be assigned to the beginning of the k-carbide precipitation. According to the phase diagram (Figure 2), these precipitates react with ferrite in the range temperature of 740–820 °C and transform into austenite by a eutectoid reaction [19–22]. This transformation ends close to 900 °C. Similarly, the reverse transformations can be assigned during the cooling process. At the beginning of the curve, the slope decreases progressively, which is related to the gradual transformation of austenite to ferrite. The peak above 900 °C can be attributed to the beginning of carbide precipitation during cooling, since at this temperature the decomposition of austenite to ferrite and k-carbide occurs through the eutectoid reaction. To study the precipitation kinetics of the k-carbides under isothermal conditions (those corresponding to an annealing treatment at a constant temperature), a permanence dilatometry test was carried out at 750 °C for 100 h. Figure 4c shows the dilatometry curve and its derivative, and Figure 4d shows a detail of the first two hours of heating. Although it is difficult to differentiate the part corresponding to the test regulation itself and homogenization of the temperature in the specimen from the part corresponding to the phase transformation, the precipitation of k-carbides seems, apparently, to take place during the first hour of maintenance.
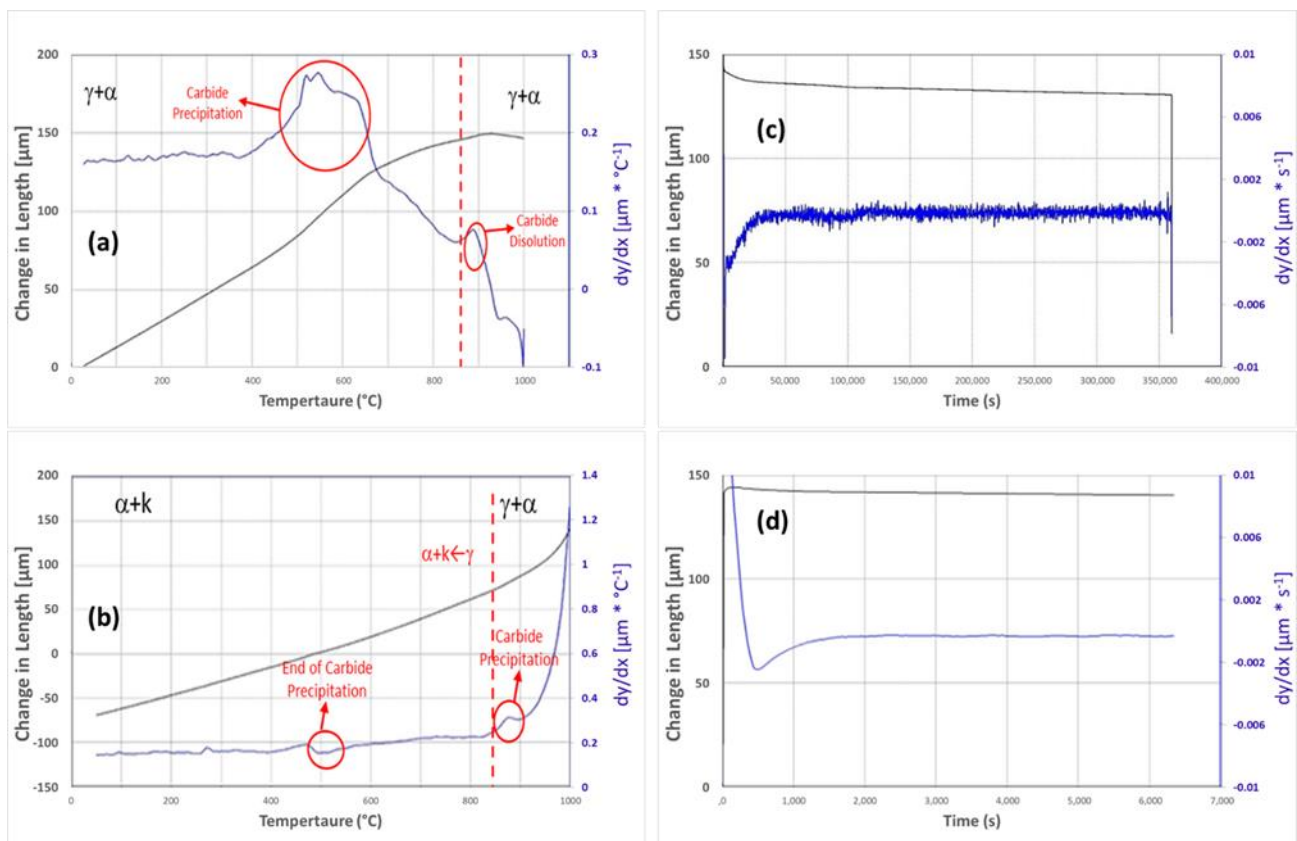
Figure 4. Dilatometry tests. (**a**) The curve (black) and its derivative (blue) corresponding to the heating process up to 1000 °C; (**b**) curves for the reverse cooling process; (**c**) curve (black) and its derivative (blue) corresponding to an isothermal treatment (750 °C-100 h); (**d**) detail of the beginning of the isothermal treatment. The symbols γ, α and k refer to austenite, ferrite and k-carbide phases, respectively.

3.2. K-Carbide Precipitation Kinetic Study

Based on the results obtained from the dilatometry test carried out at 750 °C, the effect of the holding time on the k-carbide precipitation was studied. Heat treatments were performed in a furnace. The samples were heated up to 750 °C while varying the holding times to 0.5, 1, 2 and 5 h and were finally water-quenched. Figure 5 shows the optical microscope and SEM micrographs obtained for each treatment with their corresponding XRD diffractograms. At 750 °C, the precipitation of the k-carbides begins at around 30 min. The precipitates mainly formed at grain boundaries, growing from those locations into the austenite phase. The lamellar structure suggests that the eutectoid transformation reported by other authors [19–22] is occurring. After a 1 h treatment, optical microscope micrographs confirm that the transformation is significant, and it is slightly detected by XRD. Regarding the accuracy of the XRD test under experimental conditions, it can be stated that k-carbide precipitation is lower than 0.5% for a heat treatment shorter than 1 h. As the holding time rises up to 2 h or more, the austenite peak decreases and k-carbide peak increases. After two hours, the progress of the transformation is high, while in Figure 6 the SEM analysis confirms that small austenite islands remain in the microstructure, in agreement with the corresponding diffractogram. After 5 h at 750 °C, the transformation is mostly completed, the peak corresponding to austenite has completely disappeared from the diffractogram, and SEM confirms that only residual grains of austenite remain in the material.
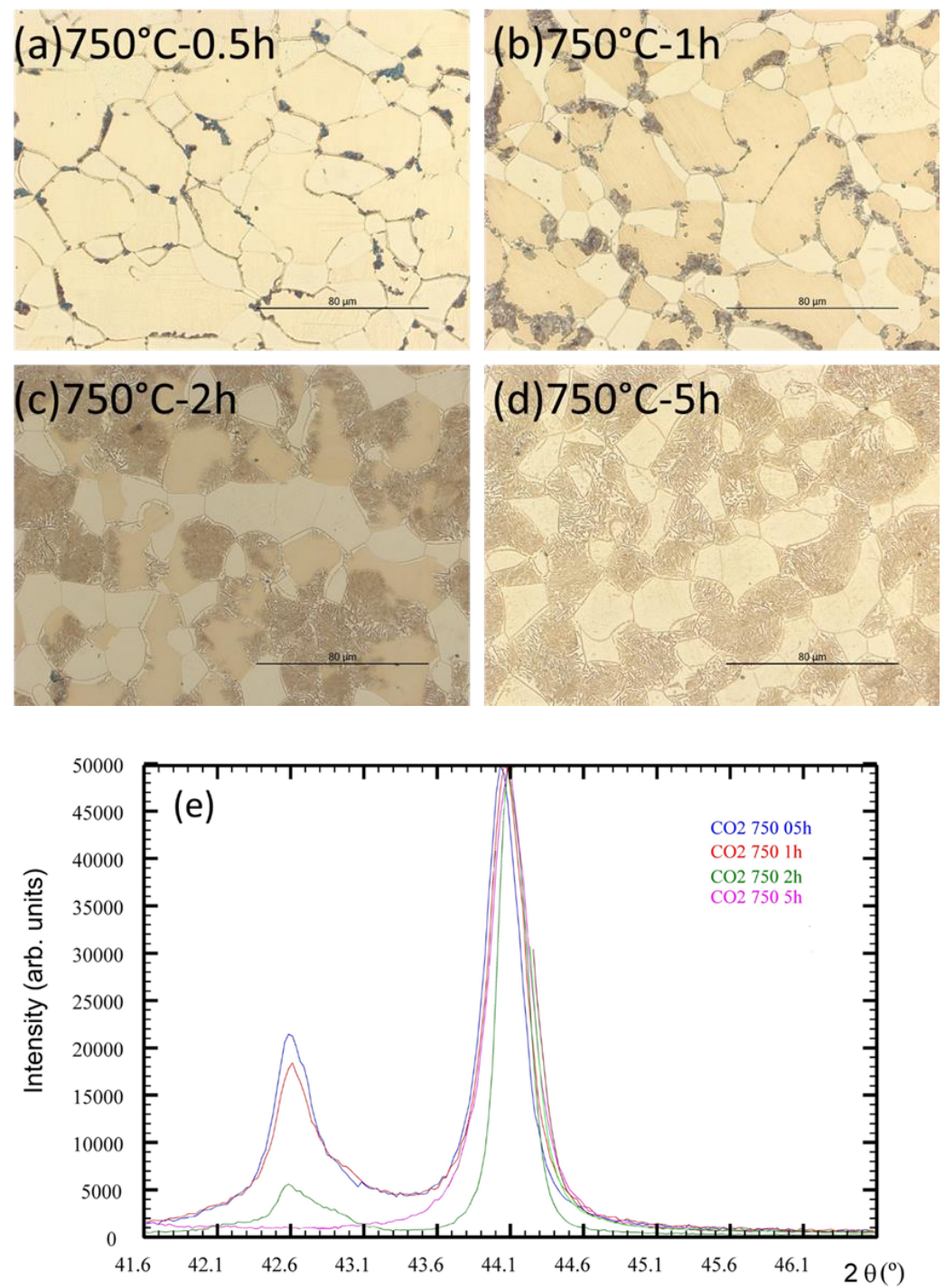
Figure 5. Optical microscope micrographs of the alloy after heat treatments performed at 750 °C for (**a**) 0.5 h, (**b**) 1 h, (**c**) 2 h and (**d**) 5 h. (**e**) Their corresponding diffractograms.
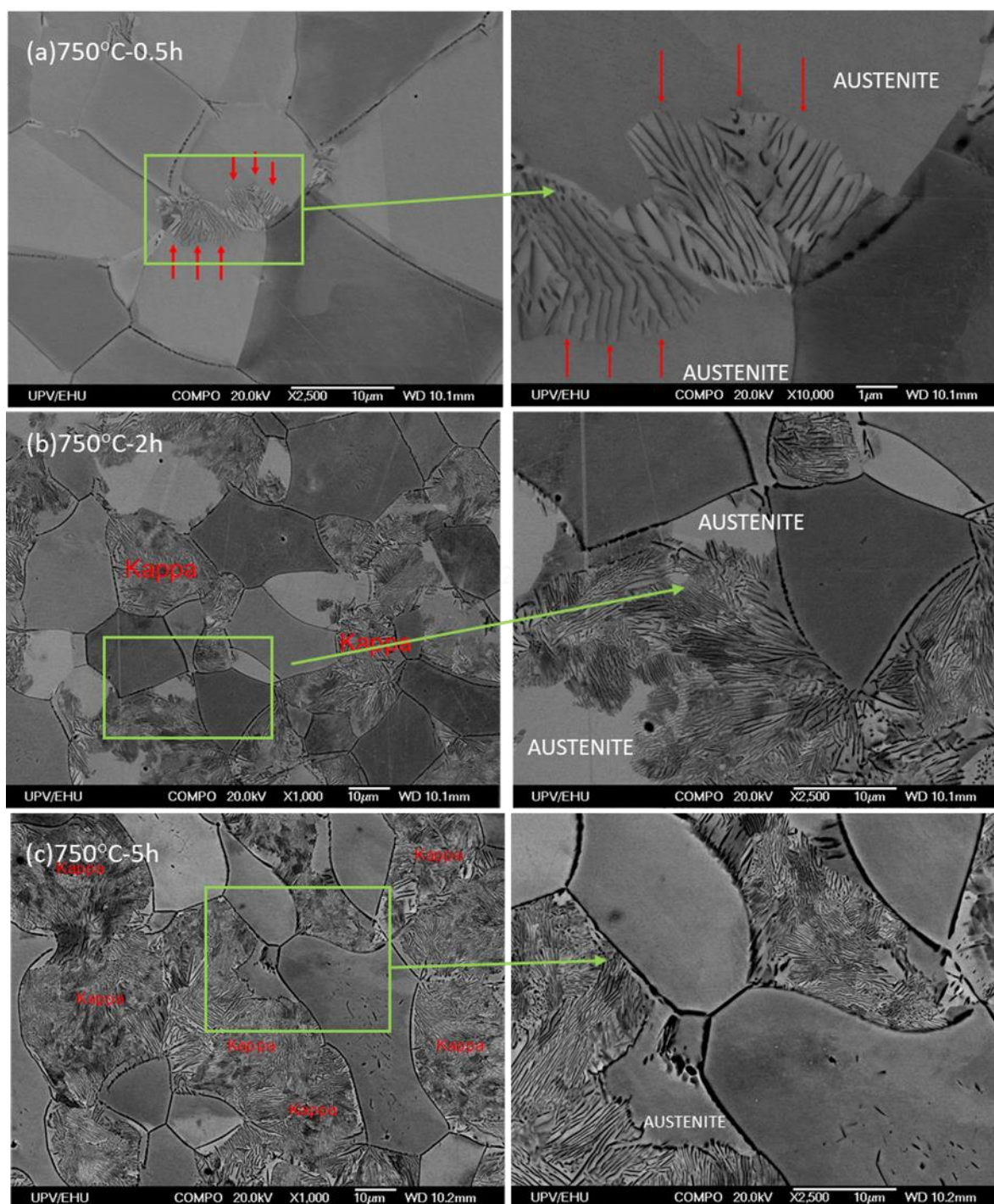
Figure 6. SEM micrographs of the alloy after heat treatments performed at 750 °C for (**a**) 0.5 h, (**b**) 2 h and (**c**) 5 h.

In order to study the influence of temperature in the first stages of k-carbide precipitation, additional treatments were performed at 700 °C and 650 °C with a holding time of 2 h. Temperatures were selected inside the range predicted by Thermocalc Software for the existence of k-carbides. Figure 7 shows the diffractograms and optical microscope images for the material after these treatments. In Figure 8's SEM images, tiny precipitates at the austenite-ferrite grain boundaries can be seen growing into the austenite phase at 650 °C. These precipitates are slightly larger at 700 °C and remain undetectable in XRD.

Taking into account the obtained results, a longer holding time of 5 h was considered for those temperatures, that is to say for 650 °C and 700 °C. All diffractograms corresponding to this holding time, shown in Figure 9, present a k-carbide peak at 40.5° and a progressive reduction of the austenite phase peak. The progress of the eutectoid transformation is depicted in the optical microscope images, where a reduction of the amount of this phase progresses as the temperature rises from 650 °C to 700 °C and 750 °C.

Table 1 summarizes whether k-carbides were identified by the analytic techniques applied for each isothermal treatment (under the testing conditions, the XRD limit detection is about 0.5% vol). Moreover, the most remarkable findings obtained from this study are:

- The precipitation of k-carbides begins at the grain boundaries, mostly austenite-ferrite, and progresses into austenite grains.
- K-carbides form from austenite decomposition into ferrite and k-carbides, resulting in a recognizable eutectoid lamellar structure. In these microstructures, primary and eutectoid ferrite are clearly distinguishable.
- At 750 °C, the precipitation of k-carbides begins after 30 min and ends at about 5 h, when approximately all the austenite has transformed into ferrite and k-carbide.
- For the same holding time, as the temperature decreases, the k-carbide precipitation kinetic slows down.
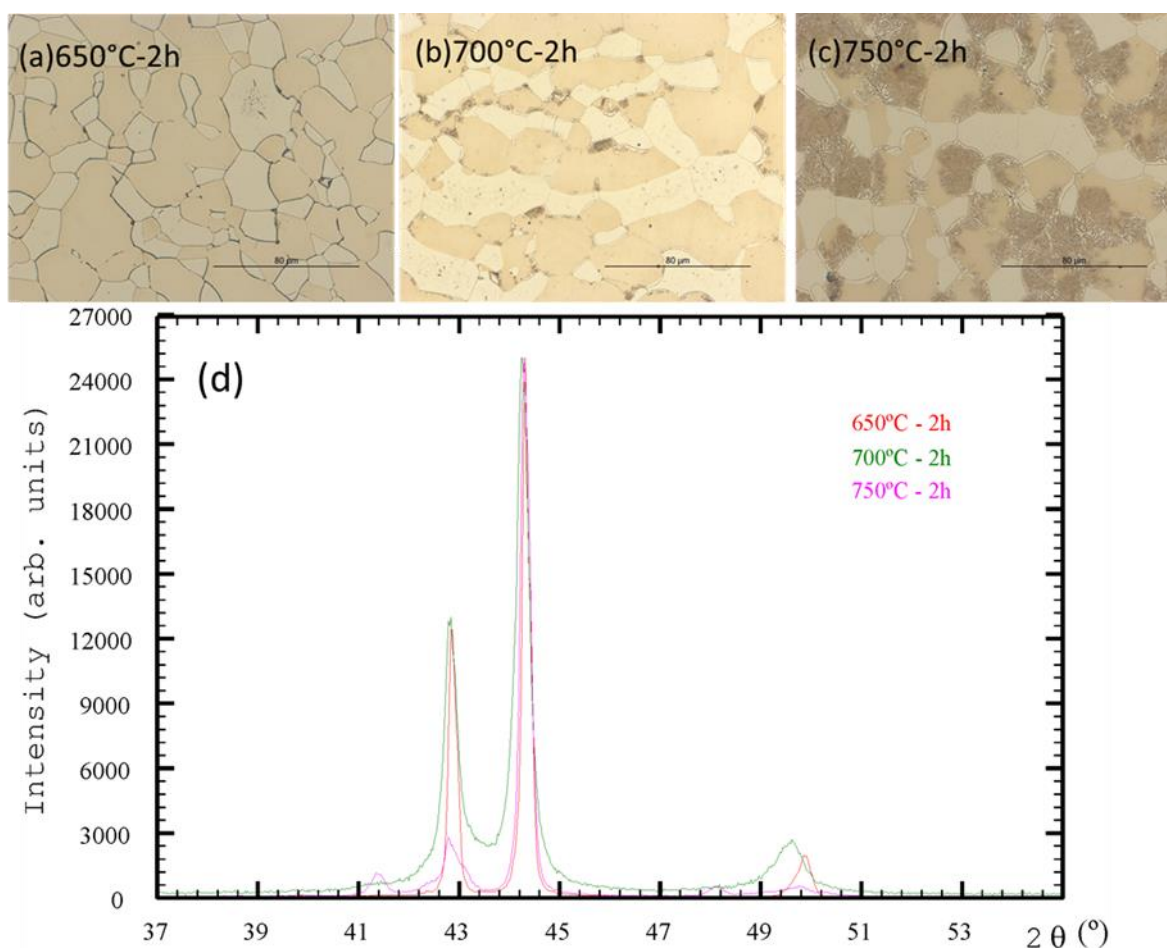

Figure 7. Optical microscope micrographs of the alloy after heat treatments performed for 2 h at (**a**) 650 °C, (**b**) 700 °C and (**c**) 750 °C. In (**d**), their corresponding diffractograms are shown.
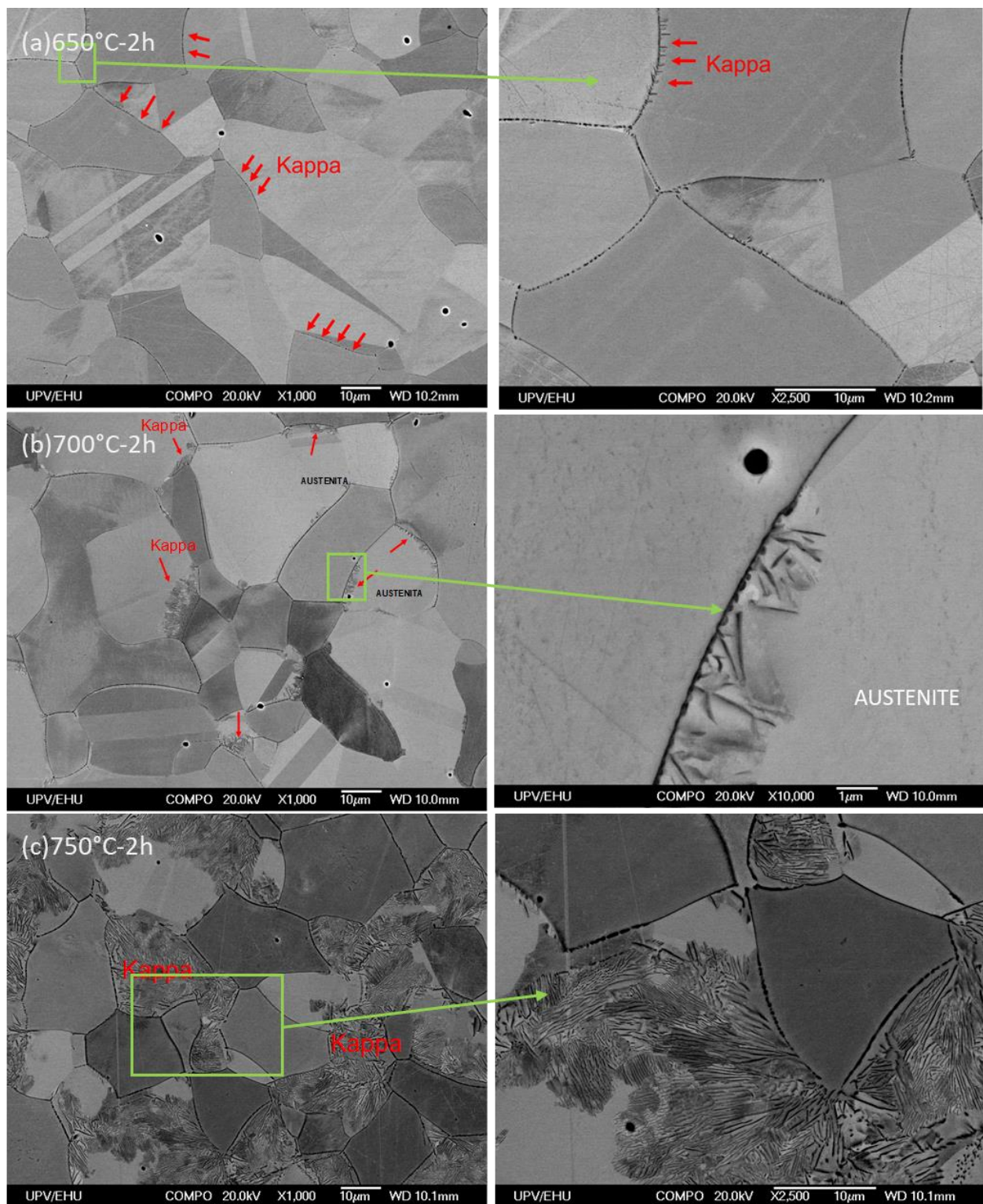
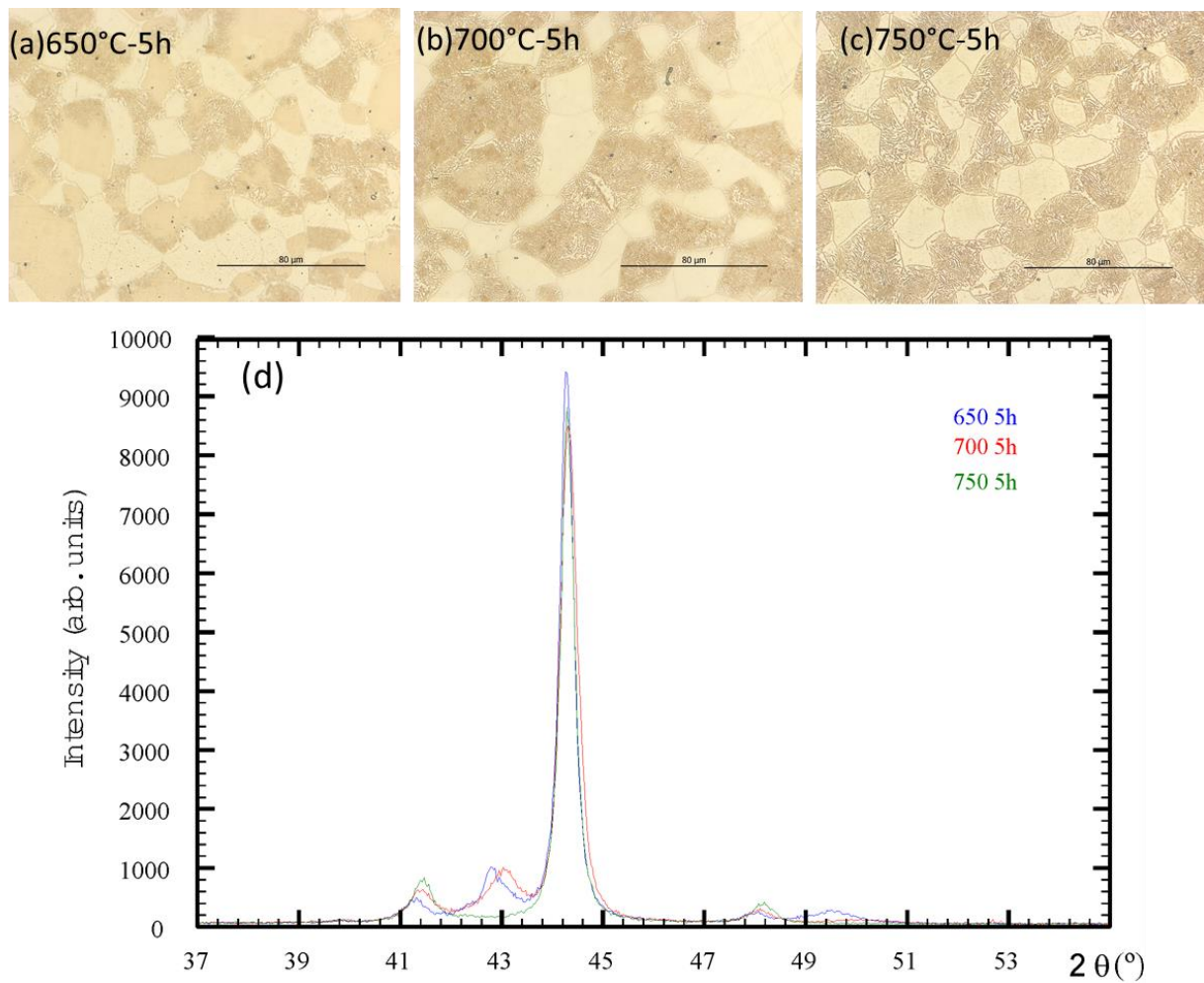**Figure 8.** SEM micrographs of the alloy after 2 h of heat treatment at (**a**) 650 °C, (**b**) 700 °C and (**c**) 750 °C.

Figure 9. Optical micrographs of the alloy after 5 h of heat treatment at (**a**) 650 °C, (**b**) 700 °C and (**c**) 750 °C. In (**d**), their corresponding diffractograms are shown.

Table 1. Applied isothermal heat treatments and results from the detection of Kappa carbides using XRD, Optical Microscope and SEM.

QT	HEAT TREATMENT		SAMPLE CODE	Kappa XRD	Kappa (OM, SEM)
	Temperature (°C)	Time (h)			
1150 °C	750 °C	0.5	750 °C-0.5 h	NO	YES
		1	750 °C-1 h	YES	YES
		2	750 °C-2 h	YES	YES
		5	750 °C-5 h	YES	YES
	700 °C	2	700 °C-2 h	NO	YES
		5	700 °C-5 h	YES	YES
	650 °C	2	650 °C-2 h	NO	YES
		5	650 °C-5 h	YES	YES

3.3. Study of the Influence of K-Carbides on the Mechanichal Properties

Regarding the microstructures obtained from the performed heat treatments, the following ones were selected to produce samples for mechanical testing:

- Ferrite and austenite formed during water quenching from 1150 °C.
- Ferrite and austenite with an initial precipitation of k-carbides formed at 750 °C for 1 h.
- Ferrite and austenite with a partial transformation of austenite into lamellar ferrite plus k-carbide, formed at 750 °C for 2 h and at 650 and 700 °C for 5 h.
- Ferrite and lamellar ferrite plus k-carbide, formed from the complete transformation of austenite performed at 750 °C for 5 h.

Minicylindrical tensile specimens of samples treated in the mentioned conditions, with a calibrated length of 30 mm, were machined and tested following the UNE-EN ISO 6892-1B:2010 standard. Figure 10 shows the tensile curves obtained for each treatment, and Table 2 summarizes the values of the mechanical properties obtained.
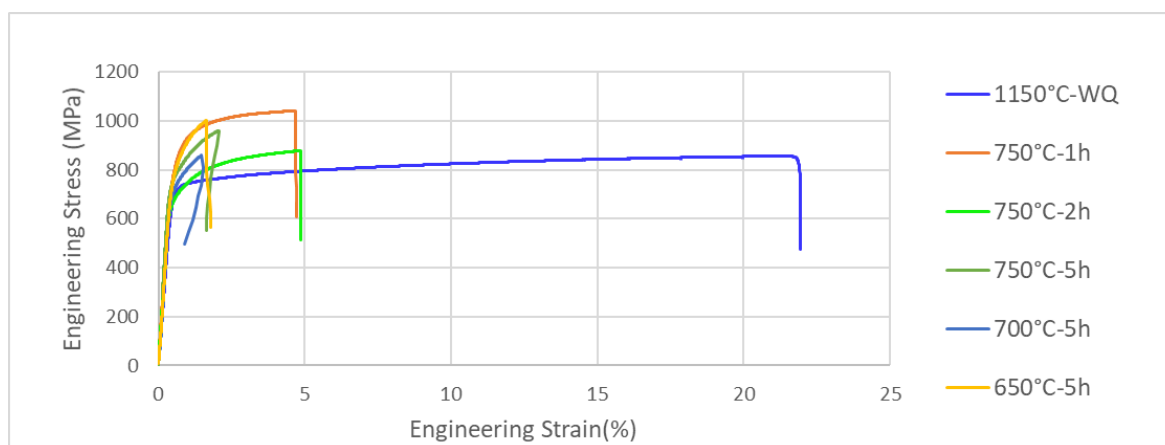

Figure 10. Tensile curves obtained for each heat treatment.

Table 2. Mechanical properties obtained for the different treatments.

HEAT TREATMENT				MECHANICAL PROPERTIES			
QT	ISOTHERMAL		SAMPLE CODE	YS (MPa)	UTS (MPa)	El (%) A30	TSxEl (GPa)
	T(°C)	Time(h)					
1150 °C	QUENCHING		1150 °C -WQ	720	855	22.1	18.9
1150 °C	750 °C	1	750 °C-1 h	838	1041	4.7	4.9
1150 °C		2	750 °C-2 h	709	878	4.88	4.28
1150 °C		5	750 °C-5 h	777	959	2.05	1.96
1150 °C	700 °C	5	700 °C-5 h	762	943	3.5	3.3
1150 °C	650 °C	5	650 °C-5 h	803	1001	1.5	1.5

From the mechanical test results, it can be concluded that the quenched sample has a greater elongation than those submitted to isothermal heat treatment and analyzed in this work. It also has the best Resistance x Elongation product value. Applying the isothermal treatments defined in this work and based on the results obtained from the ThermoCalc simulations and dilatometry tests, k-carbide precipitation is promoted and the presence of k-carbides noticeably increases the resistance of the material when compared to the quenching treatment. However, the precipitation of coarse k-carbides in the grain boundaries leads to a very poor ductility: the higher the degree of transformation, the lower the deformation to fracture. It has been reported [3] that k-carbides contribute to the enhancement of elongation when their size, shape and distribution are optimally controlled during hot working and heat treatments. From our results, it was observed that when k-carbides grew over a nanoscale size and in the grain boundaries, their contribution to

mechanical properties maintained high levels of resistance, but the elongation to fracture decreased dramatically when compared to the quenched material.

Finally, to investigate the influence of the k-carbides and final microstructures on the fracture modes, two of the tested samples were selected in order to analyze the type of fracture: On the one hand, the sample that provided the greatest elongation and the best balance of properties (1150 °C-WQ) and, on the other hand, the sample that provided the greatest resistance but a very low elongation (750 °C-1 h). Figure 11 shows the fractographies obtained by SEM of the two tested samples that were selected. In the sample that was quenched from 1150 °C, some areas of ductile breakage at the grain limit were observed, while in the sample subjected to the isothermal treatment, a crack propagating along the grain boundaries was observed, showing an intergranular fracture mode, which could be attributed to the precipitation of brittle k-carbides close to the grain limits [23]. These precipitates deteriorate the cohesion of the grain boundaries, leading to an intergranular fracture [24] and resulting in an extremely low ductility.
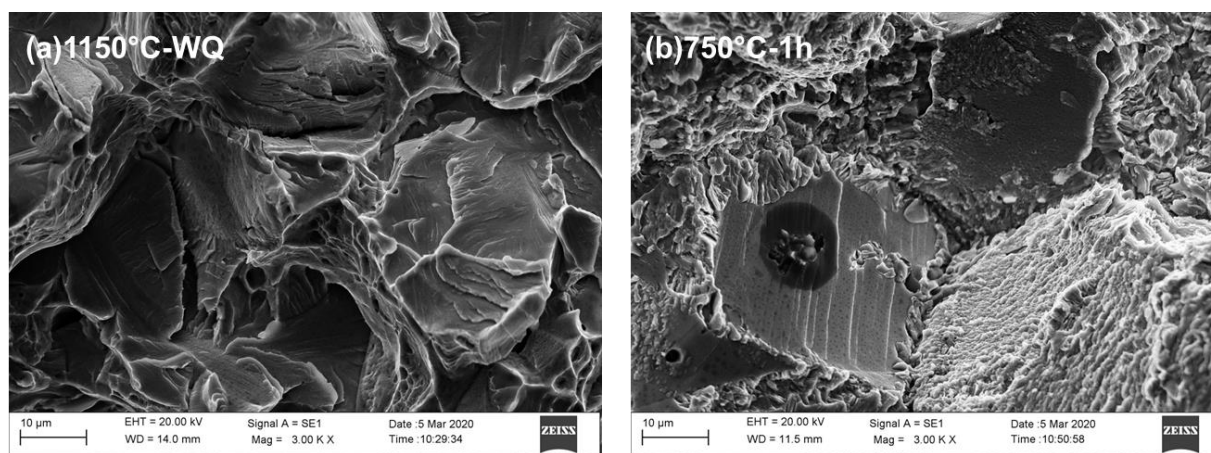

Figure 11. Fractography images obtained after mechanical tests of the samples that were (**a**) water-quenched from 1150 °C and (**b**) treated at 750 °C for one hour.

4. Conclusions

In this study, it has been observed that for austenitic duplex steels, such as the 0.66C11.4Mn9.9Al composition that was analyzed in this investigation, heat treatments that promote the precipitation of coarse kappa carbides at the grain limit can apparently increase the strength of the material when compared to a quenching treatment but cause a very detrimental effect on its ductility. For a good combination of resistance and ductility, more heat treatments must be analyzed. These heat treatments can be: isothermal heat treatments at lower temperatures or with shorter times, in order to control the size, morphology and distribution of the kappa carbide precipitates; or different temperature quenching/normalization treatments that can improve the ductility or resistance of steel while avoiding the precipitation of k-carbide.

The great potential of these low-density steels to forge components justifies their study, and further investigations must be carried out.

Author Contributions: I.K., T.G. (Teresa Gutierrez) and T.G. (Teresa Guraya) wrote the paper. All the authors conceived and designed the experiments; R.E. performed the dilatometric tests; P.J. performed the optical and electron microscope experiments. All authors discussed and reviewed the paper. All authors have read and agreed to the published version of the manuscript.

Data Availability Statement: The data are not publicly available.

Conflicts of Interest: The authors declare no conflict of interest.

References

1. Kim, H.; Suh, D.-W.; Kim, N.J. Fe-Al-Mn-C lightweight structural alloys: A review on the microstructures and mechanical properties. *Sci. Technol. Adv. Mater.* **2013**, *14*, 1–11. [CrossRef] [PubMed]
2. Chen, S.; Rana, R.; Haldar, A.; Ray, R.K. Current state of Fe-Mn-Al-C low density steels. *Prog. Mater. Sci.* **2017**, *89*, 345–391. [CrossRef]
3. Frommeyer, G.; Brüx, U. Microstructures and mechanical properties of high strength Fe-Mn-Al-C lightweight triplex steels. *Steel Res. Int.* **2006**, *77*, 627–633. [CrossRef]
4. Rana, R.; Liu, C.; Ray, R.K. Evolution of microstructure and mechanical properties during thermomechanical processing of a low-density multiphase steel for automotive application. *Acta Mater.* **2014**, *75*, 227–245. [CrossRef]
5. Haa, M.C.; Koob, J.-M.; Leeb, J.-K.; Hwanga, S.W.; Parka, K.-T. Tensile deformation of a low density Fe–27Mn–12Al–0.8C duplex steel in association with ordered phases at ambient temperature. *Mater. Sci. Eng. A* **2013**, *586*, 276–283. [CrossRef]
6. Cheng, P.; Li, X.; Yi, H. The k-Carbides in Low-Density Fe-Mn-Al-C Steels: A Review on Their Structure, Precipitation and Deformation Mechanism. *Metals* **2020**, *10*, 1021. [CrossRef]
7. Chin, K.; Lee, H.; Kwak, J.; Kang, J.; Lee, B. Thermodynamic calculation on the stability of (Fe,Mn)3AlC carbide in high aluminum steels. *J. Alloys Compd.* **2010**, *505*, 217–223. [CrossRef]
8. Jiménez, J.A.; Frommeyer, G. The ternary iron aluminum carbides. *J. Alloys Compd.* **2011**, *509*, 2729–2733. [CrossRef]
9. Lu, W.J.; Zhang, X.F.; Qin, R.S. Structure and properties of k-carbides in duplex lightweight steels. *Ironmak. Steelmak.* **2015**, *42*, 626–631. [CrossRef]
10. Grässel, O.; Frommeyer, G. Effect of martensitic phase transformation and deformation twinning on mechanical properties of Fe–Mn–Si–AI steels. *Mater. Sci. Technol.* **1998**, *14*, 1213–1217.
11. Frommeyer, G.; Jiménez, J.A. Structural superplasticity at higher strain rates of hypereutectoid Fe-5.5Al-1Sn-1Cr-1.3C steel. *Metall. Mater. Trans. A* **2005**, *36*, 295–300. [CrossRef]
12. Kim, K.-H.; Lee, J.-S.; Lee, D.-L. Effect of silicon on the spheroidization of cementite in hypereutectoid high carbon chromium bearing steels. *Met. Mater. Int.* **2010**, *16*, 871–876. [CrossRef]
13. Raabe, D.; Springer, H.; Gutierrez-Urrutia, I.; Roters, F.; Bausch, M.; Seol, J.-B.; Koyama, M.; Choi, P.-P.; Tsuzaki, K. Alloy Design, Combinatorial Synthesis, and Microstructure–Property Relations for Low-Density Fe-Mn-Al-C Austenitic Steels. *JOM* **2014**, *66*, 1845–1856. [CrossRef]
14. Seol, J.B.; Jung, J.E.; Jang, Y.W.; Park, C.G. Influence of carbon content on the microstructure, martensitic transformation and mechanical properties in austenite/ε-martensite dual-phase Fe–Mn–C steels. *Acta Mater.* **2013**, *61*, 558–578. [CrossRef]
15. Gutierrez-Urrutia, I.; Raabe, D. Influence of Al content and precipitation state on the mechanical behaviour of austenitic high-Mn low-density steels. *Scr. Mater.* **2013**, *68*, 343–347. [CrossRef]
16. Choi, K.; Seo, C.-H.; Lee, H.; Kim, S.K.; Kwak, J.H.; Chin, K.G.; Park, K.-T.; Kim, N.J. Effect of aging on the microstructure and deformation behaviour of austenite base lightweight Fe–28Mn–9Al–0.8C steel. *Scr. Mater.* **2010**, *63*, 1028–1031. [CrossRef]
17. Kaltzakorta, I.; Gutierrez, T.; Elvira, R.; Guraya, T.; Jimbert, P. Low density steel for forging. *Mater. Sci. Forum* **2018**, *941*, 287–291. [CrossRef]
18. ASTM E562-08. *Standard Test Method for Determining Volume Fraction by Systematic Manual Point Count*; ASTM International: West Conshohocken, PA, USA, 2008. [CrossRef]
19. Cheng, W.C. Phase transformations of an Fe-0.85C-17.9Mn-7.1Al austenitic steel after quenching and annealing. *JOM* **2014**, *66*, 1809–1820. [CrossRef]
20. Song, H.; Yoo, J.; Kim, S.H.; Sohn, S.S.; Koo, M.; Kim, N.J.; Lee, S. Novel ultra-high-strength Cu-containing medium-Mn duplex lightweight steels. *Acta Mater.* **2017**, *135*, 215–225. [CrossRef]
21. Jeong, J.; Lee, C.-Y.; Park, I.-J.; Lee, Y.-K. Isothermal precipitation behaviour of κ-carbide in the Fe–9Mn–6Al–0.15C lightweight steel with a multiphase microstructure. *J. Alloys Compd.* **2013**, *574*, 299–304. [CrossRef]
22. Zhao, C.; Song, R.; Zhang, L.; Yang, F.; Kang, T. Effect of annealing temperature on the microstructure and tensile properties of Fe-10Mn-10Al-0.7C low-density steel. *Mater. Des.* **2016**, *91*, 348–360. [CrossRef]
23. Meng, S.; Sugiyama, S.; Yanagimoto, J. Effects of heat treatment on microstructure and mechanical properties of Cr-V-Mo steel processed by recrystallization and partial melting method. *J. Mater. Process. Technol.* **2014**, *214*, 87–96. [CrossRef]
24. Raabe, D.; Herbig, M.; Sandlöbes, S.; Li, Y.; Tytko, D.; Kuzmina, M.; Ponge, D.; Choi, P.-P. Grain boundary segregation engineering in metallic alloys: A pathway to the design of interfaces. *Curr. Opin. Solid State Mater. Sci.* **2014**, *18*, 253–261. [CrossRef]